Journal of The British Interplanetary Sociey, Vol. 43, pp.209-216, 1990

A METHOD FOR SEARCHING FOR ARTIFICIAL OBJECTS ON PLANETARY SURFACES

MARK J. CARLOTTO and MICHAEL C. STEIN
The Analytic Sciences Corporation, 55 Walkers Brook Drive, Reading, MA 01867, USA.

The focus of the search for extra-terrestrial intelligence (SETI) has been to detect radio frequencies emanating from outside our Solar System for signs of intelligent life. This strategy is consistent with current information which suggests it is unlikely that intelligent life has evolved on the other planets in our solar system. However, the possibility that extra-terrestrials or their probes may have reached this solar system cannot be ruled out. If so, they may have altered planetary surfaces in ways detectable by remote sensing. An alternative strategy is proposed for a systematic search for anomalous, i.e., possible non-natural objects on planetary surfaces. An approach for detecting anomalous objects in planetary imagery based on the fractal modelling of planetary terrain is described. Viking orbiter imagery suggest that certain objects on the Martian surface currently under investigation may not be natural. Preliminary results of applying the technique to Viking orbiter imagery suggest that certain objects on the Martian surface may not be natural.

1. INTRODUCTION

The search for extraterrestrial (ET) intelligences at radio frequencies began with project Ozma [1] but has produced no evidence for their existence. The success of such an endeavour requires that:

(1) there are advanced technological civilisations in the galaxy either communicating with one another or trying to communicate with us,

(2) it is possible to detect their signals, and

(3) such signals can be deciphered when received.

The Drake equation [2] has been a starting point for speculating on the number of technological civilisations in the galaxy. One extreme maintains that ours is the only advanced civilisation in the galaxy for, if there were others, evidence of their existence would be available (the Fermi Paradox). The other extreme maintains that there are billions of advanced technological civilisations in the galaxy. Evidence in favour of either extreme is scarce. Estimates derived from the Drake equation depend on parameter values which are obviously based on limited knowledge. Freitas [3] argues that the Fermi Paradox cannot be proven. The present consensus is that the number of advanced civilisations lies between the two extremes and is sufficient to warrant some kind of search.

Many believe that the best channel for ET communications is at 1420 MHz, the frequency at which atomic hydrogen radiates [4]. Even with this starting point, as the bandwidth of spectrum analyzers decreases and the angular resolution of radiotelescopes increases, the number of frequencies and directions to be searched increases. There is a feeling that the lack of success is due to the very limited portion of the "search space" covered to date, because the technology to detect and decipher ET radio transmissions does not yet exist, or the signal is simply not there [5].

An alternative strategy involves searching for ET probes or artifacts. Freitas [6] has proposed a search for messenger probes in the vicinity of the Earth. Based on the argument that intelligent life has the natural tendency to expand into and occupy space, and requires raw materials to support such expansion, e.g., for building space colonies, Papagiannis [7] argues that if ETs are in our solar system, they may be in the asteroid belt. Using arguments similar to those based on the Drake equation, Foster [8] estimates frequencies of visitations by ETs or their messenger probes and suggests the possibility that past encounters may have left behind artifacts or indirect evidence, e.g., deranged planetary terrain.

This last idea is the point of departure for this paper, that there may be such artifacts already imaged by probes such as Viking Orbiter. For example, there is considerable interest in a collection of unusual surface features in the Cydonia region of Mars [9-12]. Is there a way to assess these and other surface features objectively so that future missions such as the Mars Observer can gather more data?

Detection criteria must be established if an objective search for artificial features is to be carried out. Current SETI strategies have been criticized on such grounds as, e.g., we are looking for what we *think* is out there [5]. We cannot define in a direct way what is "artificial" because we do not know what we are looking for. However, we can attempt to define what is natural and proceed to measure the "naturalness" of unknown features. Artificial features are then identified as those farthest, in some sense from "natural".

The contributions of this paper are fourfold:

(1) define objective criteria for identifying possible artificial objects,

(2) describe a technique based on fractal geometry for detecting such objects,

(3) present preliminary results in applying the technique to Viking orbiter imagery of unusual Martian surface features

(4) outline a strategy for continuing the search as part of on going planetary exploration programs.

2. CHARACTERISING NATURAL LANDSCAPES USING FRACTAL GEOMETRY

Mandelbrot [13] has defined a fractal as an object whose Hausdorff-Besicovitch dimension is strictly greater than its topological dimension. For example, a fractal surface in 3-d space whose topological dimension is 2 would have a fractal dimension between 2 and 3. Fractals have been shown to be good models for diverse physical and biological phenomena such as the length of coastlines, stream flow volume, terrain surface area, volume of blood vessels and many more [13]. A reason is that natural phenomena often possess the property of being self-similar at different scales or resolutions. Self-similarity is defined by the relation

$$M(rX) = r^{f(D)} M(X) \tag{1}$$

where M(X) represents any metric property of the fractal (e.g. surface area), X represents a scale of measurement of the metric property, r is a scaling factor between zero and one, and f(D) is a simple function of the fractal dimension that depends on the metric property. This equation states that the metric property computed at a reduced scale of measurement is equivalent to scaling the metric property of the fractal at the original scale implies that the metric property obeys a power law function of the scale of measurement

$$M(X) = KX^{f(D)} \tag{2}$$

where K is a constant.

For the purpose of modelling landscapes, a class of statistical fractals known as fractional Brownian motion [14] has been used extensively. Fractional Brownian surfaces may be described by their second order difference statistics,

$$\text{Variance } | B_H(t)-B_H(t+T) | \sim T^{2H} \tag{3}$$

their surface area,

$$A(r) \sim r^{2-D} \tag{4}$$

or their power spectral density,

$$S(f) \sim 1/f^{(1-2H)} \tag{5}$$

where D = 3 - H.

Equation (3) states that the variance of the difference between any two points on the fractional Brownian surface a distance T apart increases at a constant power of the distance (since $0 < H < 1$); (4) states that the surface area decreases as a constant power of the scale (since $2 < D < 3$); (5) states that the power spectral density (power per unit frequency) decreases as a constant power of the spatial frequency.

Mark and Aronson [15] analyzed 17 topographic data sets in the United States using variograms which plot variance versus distance as defined in equation (3). They found that most of the data sets could not adequately be characterised by a single fractal dimension, i.e., the logarithm of the variance was not linearly related to the logarithm of the distance over all distances or scales. Rather, the behaviour of topography tended to be divided into scale ranges. Over small scales (< 0.6 km) many of the surfaces could be modelled as fractional Brownian surfaces with D around 2.2 - 2.3. Over larger scales, higher dimensions around 2.75 were noted. At still larger scales many surfaces exhibited periodicities. A similar result was noted by Clark [16] who suggests that a combination of fractal models to model local behaviour combined with Fourier models to model longer-term variations be used for modelling topography. Locally, at least, fractals seem to be good models for topography. Clarke suggests that on planets like Mars where the types of processes that shape terrain over larger scales on Earth are absent for the most part, fractals may be adequate models by themselves. For example, Woronow [17] shows that fractals can be used as models for classifying certain kinds of large-scale Martian impact craters.

The above suggests a reason why the generation of realistic synthetic terrain using fractional Brownian motion has been so successful as demonstrated by Voss [18] and by Fournier *et al* [19].

Figure 1 is a 3-d plot of a synthetic terrain surface (D = 2.1) produced by Voss' method for generating fractional Brownian surfaces using discrete Fourier synthesis. The method is based on passing the discrete Fourier transform of a 2-d white Gaussian noise field through a linear filter with a circularly symmetric transfer function proportional to $k^{-(1+\beta)/2}$ and inverse transforming the result. Here k is discrete frequency and the fractal dimension $D = 2 + (3 - \beta)/2$.

Figure 2 shows several views of this synthetic terrain surface. A Lambertian reflectance function was used to create a shaded rendition of the terrain surface (left). The Sun is south

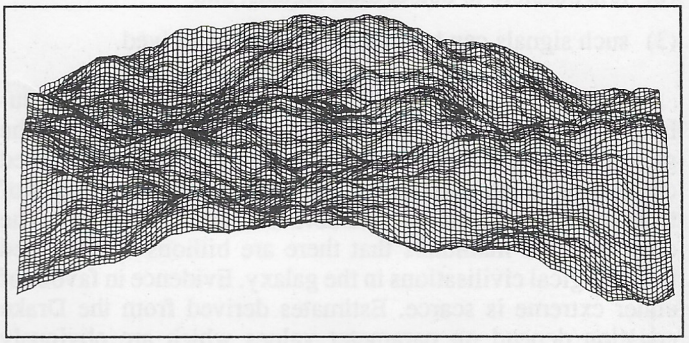

Fig. 1. 3-d plot of synthetic terrain produced by Voss' method for generating fractional Brownian surfaces (fractal dimension = 2.1).

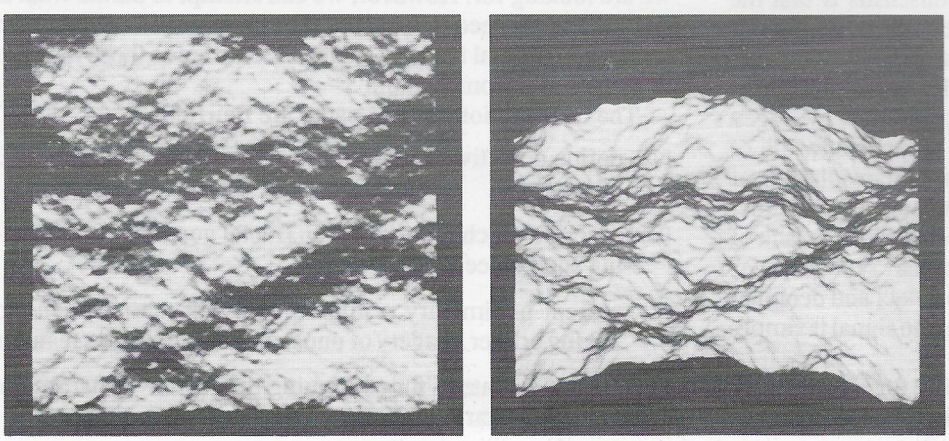

Fig. 2. Orthographic view of shaded rendition of synthetic terrain (left) and an oblique parallel projection (right).

(solar azimuth $\theta_0 = 180°$) at a zenith angle $\phi_0 = 45°$. An oblique view was then generated by viewing the shaded rendition mapped on to the elevation surface via an oblique parallel projection (right). The image was computed from a view at an azimuth angle $\theta_1 = 180°$ and a zenith angle $\phi_1 = 60°$.

3. DETECTING MAN-MADE OBJECTS

A major focus in artificial intelligence and machine vision has been on the problem of recognising instances of known objects in imagery [20]. The problem of recognising an unknown object as an instance of a known object or class of known objects involves comparing features of the unknown object that can be computed from the available data to those of known objects and selecting the object with the best match.

The problem of recognising unknown or unexpected objects, and the related problem of detecting man-made objects embedded in natural terrain, are fundamentally different. One possible approach might be to determine the characteristics that are common to all man-made objects. For example, one thinks of man-made objects as having flat surfaces, sharp boundaries and different brightness from the background. Unfortunately, due to lighting conditions, imaging geometry, and obscuration, the strong linear features that one might expect are often not there.

An alternative approach based on modelling the background has recently been proposed by Stein [21]. The approach does not rely on an explicit model for man-made objects, e.g., that they are rectangular in shape or brighter than the background. Rather, it is based on the observation that man-made objects tend not to be self-similar in structure and so fractals should be poor models for man-made objects.

The method is based on estimating the fractal dimension of the image intensity surface within a rectangular "window" that is about the size of the objects one would like to detect, along with the error that results from assuming fractal of self-similar behaviour. The technique used to estimate the fractal dimension involves computing the surface area A(r) of the image intensity surface as a function of scale r (Appendix A). The metric properties of self-similar sets scale according to a power law as noted in (2). The fractal dimension of the image intensity surface is estimated by performing a linear regression of log A(r) over log r. A measure of the degree to which the image intensity surface lacks self-similarity; is estimated by summing the residuals of the linear regression over scale, i.e.,

$$\varepsilon = \sum_r \left| \log A(r) - (2-D) \log r \right|. \qquad (6)$$

Surfaces that are not self-similar will not follow a power law relationship, hence the residuals in (6) will be large and so will be large.

An entire image is processed by repeating the above process on a pixel-by-pixel basis within a "sliding window". Two images are produced. One is the local fractal dimension D(x,y), i.e., the fractal dimension of the portion of the image intensity surface within the rectangular window centered at (x,y); the other is the local fractal model-fit image $\varepsilon(x,y)$. The example shown in Fig. 3 is an image of military vehicles embedded in natural terrain (upper left). The results show that the parts of the image containing vehicles have a higher fractal dimension (upper right) and fractal model fit error(lower left) than the background, as predicted by the model.

For natural textures on Earth, typical ranges can be used for thresholding the fractal dimension image to generate detections. At the upper end, terrestrial observations by Mark and Aronson [15] indicate that fractal dimensions over short scales are less than about 2.5. At the low end, it has been observed that discontinuities in the image intensity surface, e.g., due to shadows, object boundaries, and obscuration produce fractal dimensions that are below the topological dimension. Thus, for detecting man-made objects, regions whose fractal dimension is not strictly greater than 2.0 and less than about 2.5 are considered anomalous.

The fractal model fit is another independent measure of anomalous behaviour. Unfortunately, since the fractal model fit

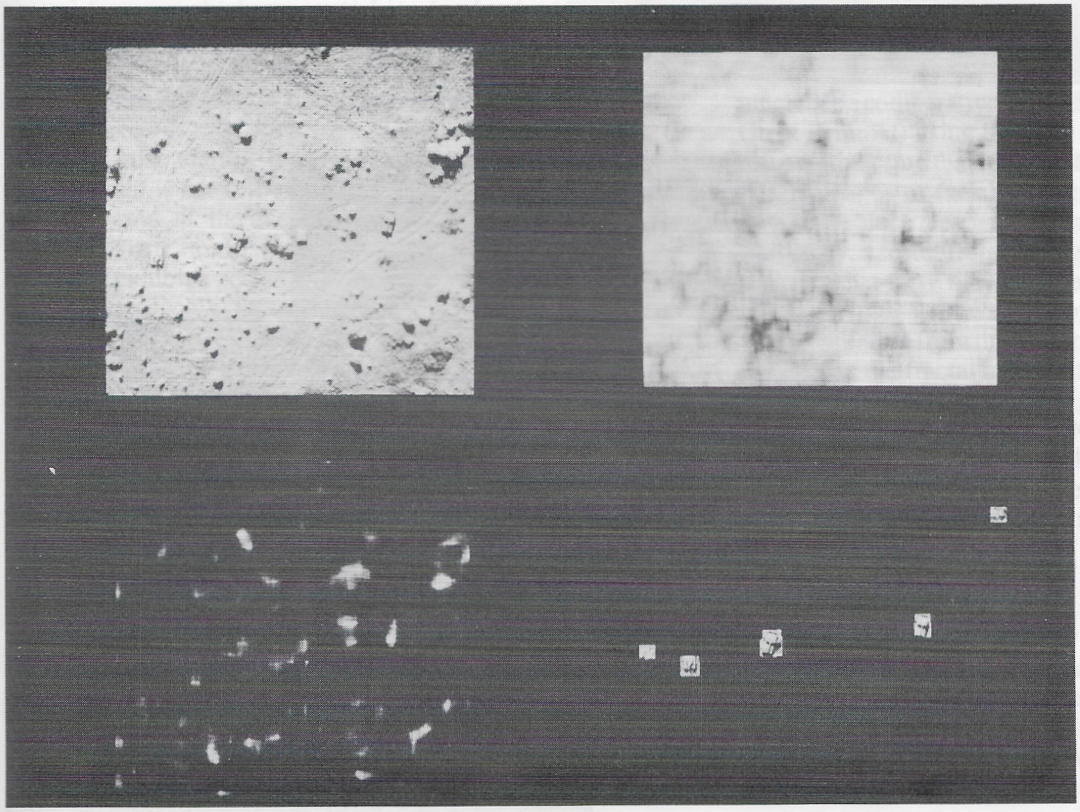

Fig. 3. Detection of man-made objects. Original image (upper left) has four military vehicles embedded in a complex natural background. Fractal dimension (upper right) and fractal model fit (lower left) images indicate that man-made objects are different than the background. Areas whose fractal dimension is outside of range $2 < D < 2.5$ and whose model fit is greater than 90%-ile are shown (lower right). The result shows 3 detections out of 4 objects with 2 false alarms.

error is a relative measure, absolute thresholds do not exist. If the relative frequency of occurrence of man-made objects is small however, the model fit image can be thresholded at a given false alarm rate (the probability that a man-made object may be detected when one is not actually present). The detection result (lwer right) in Fig. 3 indicates a possible man-made object where the fractal dimension is not between 2.0 and 2.5, and where the fractal model fit error is greater than the 90th percentile.

Limited data restricts the use of the fractal dimension for anomaly detection on Mars. For the imagery processed, the fractal dimension is used only to remove some object and shadow boundary effects by eliminating regions whose fractal dimension is less than 2.0. The unthresholded fractal model fit error image is used by itself in the remaining areas to indicate the degree to which the data lacks the self-similar behaviour of natural terrain on a local basis.

4. PRELIMINARY MARS/VIKING ORBITER RESULTS

Figure 4 is a mosaic of parts of three Viking frames: 35A72, 35A73, and 35A74. A 1280 by 1024 pixel area is shown. This is the area in Cydonia currently under study [9-12]. The resolution is about 50 metres per pixel and the total area shown in approximately 3000 km^2.

The result obtained by applying the anomaly detection technique to the imagery over this area is shown in Fig. 5. The image was produced by combining the fractal dimension and model fit images as described in the previous section. Ten scales and a 21 by 21 pixel analysis window were used. The analysis window thus covers an area about 1 km^2 and is near the upper scale limit for self-similarity based on Mark and Aronson's results for terrestrial landscapes. The "face" [9] was found to have the largest fractal model fit error which implies that it

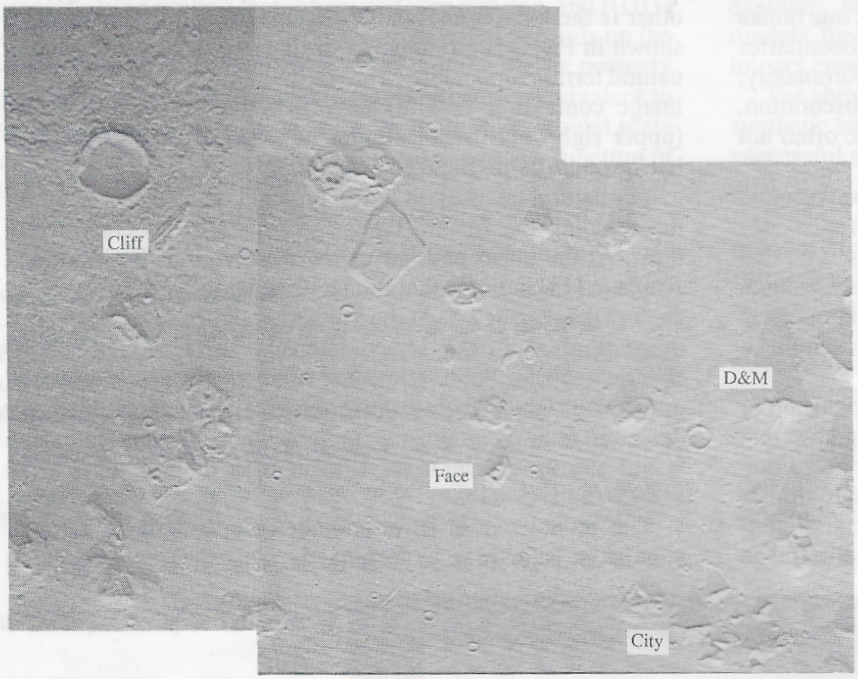

Fig. 4. Mosaic of Viking orbiter frames 35A72, 73, and 74. Landmarks shown are the "face", the "city", the "D&M pyramid", and the "cliff".

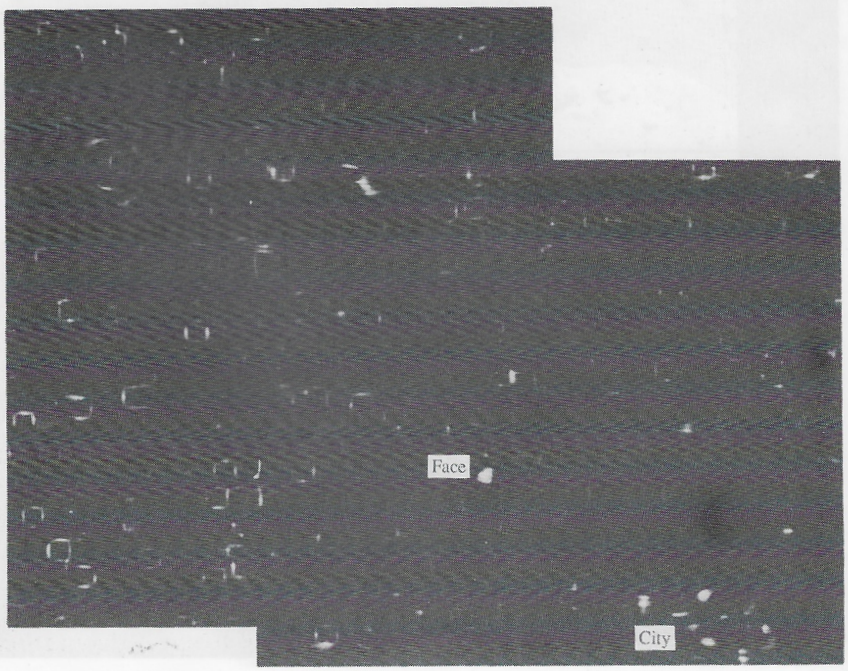

Fig. 5. Detection results show largest anomalies over the "face" and within the "city". Square rings are caused by drop-outs in the original data.

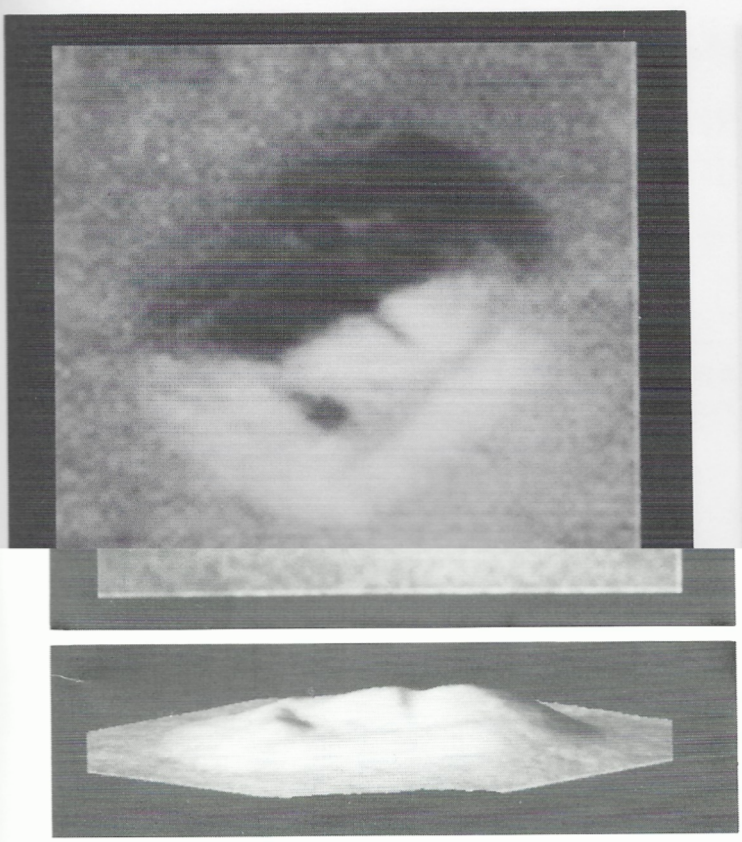

Fig. 6. Close ups of the "face": down-looking (top) and an oblique view near ground level on the Sunlit side (bottom).

is the least natural object in this area. Close-ups of the face are shown in Fig. 6. A number of objects in the "city" [11] also have large fractal model fit error. Close ups of one of those objects, the "fortress" [12] are shown in Fig. 7.

As was seen in Fig. 3 the object detection technique may indicate the presence of a man-made object when there is no such object (false alarms) and may fail to detect a man-made object when one is there (missed detections). In Figs. 4 and 5, several features which appear to be natural seem to exhibit a certain degree of non-fractal behaviour. On the other hand, several other unusual objects (e.g., the "cliff" [11] and the "D&M pyramid" [9]) do not appear to be anomalous by the technique.

As for false alarms, it is possible for nature to produce a structure that is not self-similar over short scales. In fact, this has been said of the face and the other nearby objects in Cydonia. There are many features on Mars as well as on the Earth that exhibit a periodic structure over short scales and are therefore not locally fractal.

In regard to the missed detections, it was observed earlier that images of fractal surfaces are also fractal, though the converse is not necessarily true. If a man-made object is illuminated so that its 3-d structure does not induce significant shading and shadowing effects, structural information will be lost by the image formation process. The image of the object will look smoother than it really is and will appear less anomalous. In other words, the ability to discriminate anomalous objects from the background may be reduced at certain Sun and viewing angles. This is illustrated in Fig. 8 which shows two images of the face (Viking frames 35A72 and 70A13) and surrounding terrain. In 35A72 where the Sun is more than 15° lower than in 70A13, the ability to discriminate the face from the background is much greater.

To verify that the technique does not predict a plethora of non-natural objects, it was applied to the full Viking frame

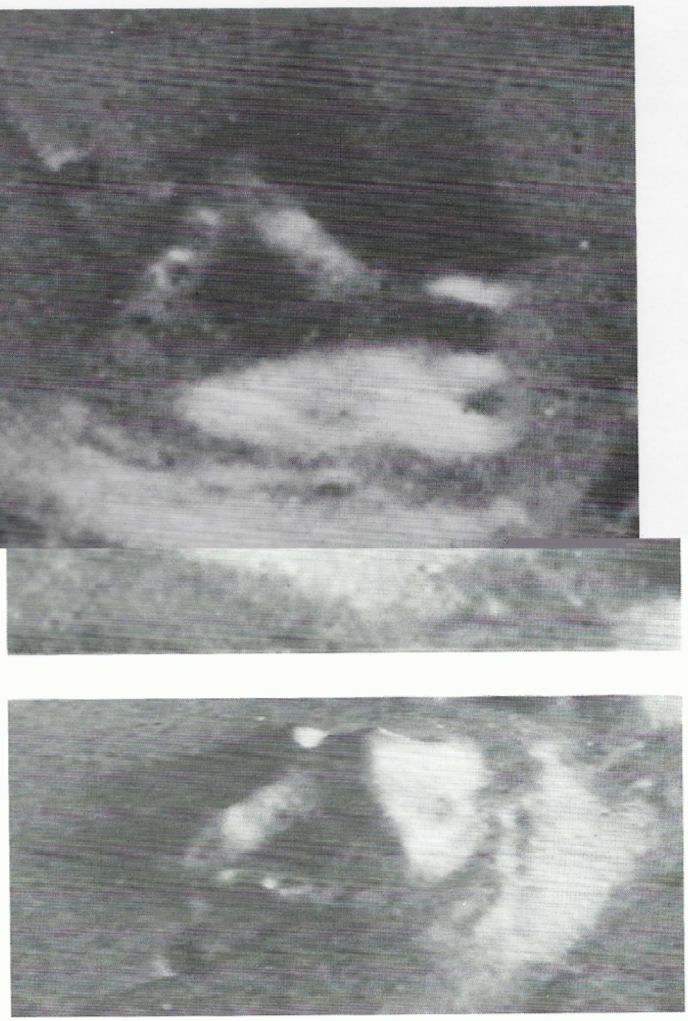

Fig. 7. Close ups of the "fortress" within the "city": down-looking (top) and an oblique view looking into the inner space (bottom).

containing the above objects (35A72) as well as three other nearby frames: 35A70, 35A71 and 35A73. The strength of the strongest detection in 35A72, the "face", was 1.75, 1.88, and 4.31 times greater than the strongest detections in these three other frames, respectively. The size of these objects (1-2 km) precludes a comparative analysis of terrestrial analogs (e.g., the Great Pyramid) using imagery such as Landsat or SPOT. It is also worth noting that it would be difficult, if not impossible to obtain images of facial profiles such as those carved on Mt. Rushmore since they were not meant to be viewed from above.

Finally, a result from Viking frame 70A10 is presented that suggests that there may be other objects on Mars worth investigating. Figure 9 shows a 512 by 512 pixel region from 70A10. It is over 100km from the Cydonia region in Fig. 4. Also, shown in Fig. 9 is the fractal model fit error image obtained with the same parameters used earlier. Ignoring the bright areas caused by periodic noise in the data, a strong anomaly is present over an unusual rectangular structure having a circular depression and a tapered "access ramp". Nearby are a pyramidal object and sharp angular features etched into the surrounding terrain.

5. SUMMARY

It is possible that there are surface features on Mars that may not be natural and warrant further investigation. In particular, higher resolution imagery must be collected e.g. by the Mars Observer in 1993. Furthermore, current thinking in the SETI community [26-28] needs to be broadened to include a system-

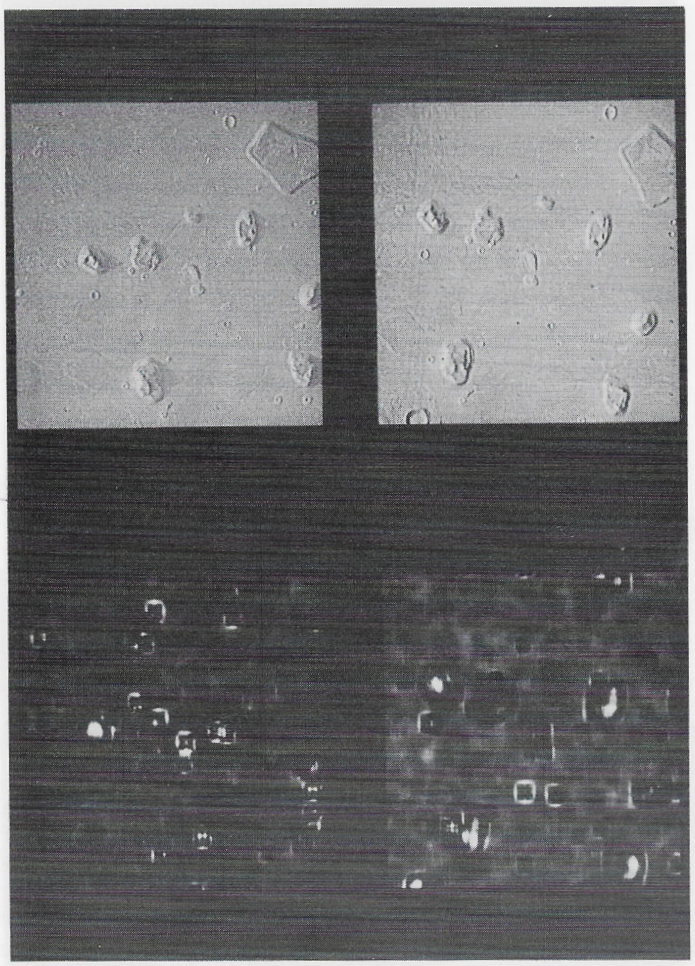

Fig. 8 Effect of illumination on the detection of anomalous features. Part of 70A13 and fractal model fit error image (top right and bottom right). Part of 35A72 and fractal model fit error image (top left and bottom left). Note the reduction in the false alarms at the higher Sun Zenith angle in 35A72. The face has the highest fractal model fit error in both images.

atic search for ET artifacts in our solar system.

The criteria and techniques discussed in this paper are a starting point for beginning an objective and systematic search for ET artifacts. It is within the state-of-the-art to process the current Viking orbiter imagery archive (about 60,000 images). Estimated costs of the order of ten million dollars to process existing planetary imagery and create an automated system for screening future imagery is many orders of magnitude less than some of the more ambitious radio search projects proposed.

ACKNOWLEDGEMENTS

The authors wish to thank Keith Hartt for the 3-d surface reconstructions used in the paper.

APPENDIX A - OBJECT DETECTION ALGORITHM

The object detection technique [21] is briefly presented here. Starting with the image, x(i,j), a series of grayscale erosions and dilations are computed

$$b_{r+1}(i,j) = \min \{b_r(i,j) - 1, b_r(i-i',j-j')\}$$
$$t_{r+1}(i,j) = \max \{t_r(i,j) + 1, t_r(i-i',j-j')\} \quad (A1)$$

where $b_0(i,j) = t_0(i,j) = x(i,j)$, $|i'| \leq 1$ and $|j'| \leq 1$. These are used

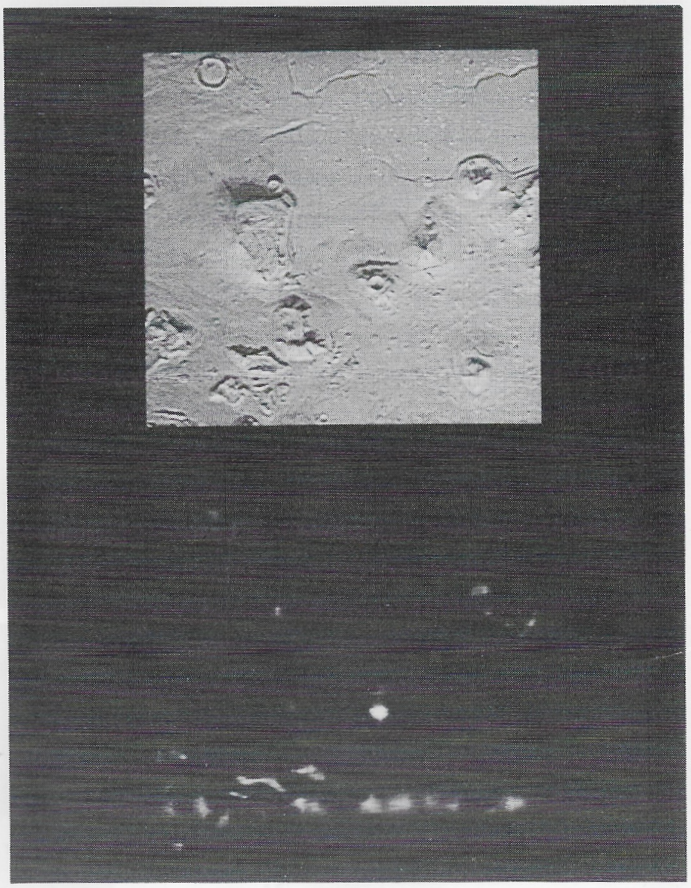

Fig. 9. Analysis of part of 70A10 frame (top). Fractal model fit error image (bottom) indicates strong anomaly over rectangular feature with central depression and v-shaped opening. Note pyramidal object and linear features above and to the right.

to compute the volume of a covering of the image intensity surface as a function of the scale parameter r:

$$v_r(i,j) = t_r(i,j) - b_r(i,j). \quad (A2)$$

to obtain an estimate of the surface area for an m x n rectangular patch centered at (i,j) the volume within a window of the same size is summed and divided by twice the scale parameter:

$$A_r(i,j) = (1/2r) \sum_{i'} \sum_{j'} v_r(i-i',j-j') \quad (A3)$$

where $|i'| < m/2$ and $|j'| < n/2$.

The fractal model is formally a linear regression model relating the logarithm of the surface area estimates $A_r(i,j)$ to the logarithm of the scale parameter r

$$\log A_r(i,j) = [2 - D(i,j)]\log r + E_r(i,j) \quad (A4)$$

where $E_r(i,j)$ is the residual of the linear fit at scale r, i.e. the difference between the predicted, using the linear model, and actual value of the logarithm of the surface area. D(i,j) is the fractal dimension and is related to the slope of the linear regression of log $A_r(i,j)$ onto log r. The fractal model fit error is the average of the squared residuals

$$\varepsilon(i,j) = (1/R) \sum_{r} E_r^2(i,j) \quad (A5)$$

where R is the number of scales.

APPENDIX B - IMAGE FORMATION MODEL

The anomaly detection technique tacitly assumes that the self-similar structure of terrain is preserved through the imaging process. Pentland [22] and Kube and Pentland [23] have analyzed the properties of images of fractal surfaces and show that under certain conditions the image of a fractal Brownian surface is also fractal Brownian, and hence, self-similar.

The simplified model of the image formation process shown in Fig. B1 was used to verify experimentally that images of fractal surfaces are also fractal. The model ignores atmospheric effects and sensor degradation. It assumes a single point source (the Sun), a Lambertian surface reflectance function, constant albedo, and an imaging sensor that is far enough away for a parallel projection to hold. These assumptions appear to be reasonable over small areas on Mars under limited illumination and viewing conditions [12]. A computational model of the image formation process can be divided into two parts:

(1) computing a shaded rendition of the surface, and,

(2) projecting the shaded surface onto the focal plane of the imaging sensor.

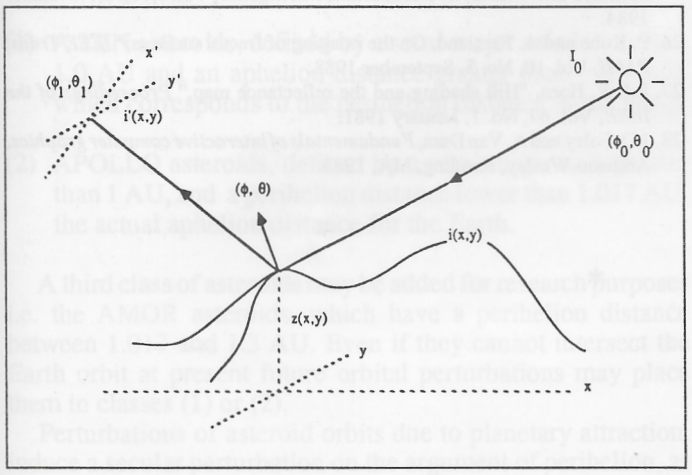

Fig. B1. Image formation model. Shaded rendition i(x,y) is a function of the reflectance properties of the surface and the position of the light source. An oblique view i'(x',y') is generated by a parallel projection.

The shaded rendition i(x,y) is related to the elevation surface z(x,y) by the reflectance map R(p,q) where the gradients p = dz(x,y) /dx and q = dz(x,y)/dy are the partial derivatives of the elevation in the x and y directions. The reflectance map depends on the reflectance properties of the surface and on the position of the Sun and the viewer. The use of the relectance map in computing shaded renditions of terrain is discussed by Horn [24]. The location of the Sun in "gradient space" is (p_0,q_0) where $p_0 = \tan \phi_0 \cos \theta_0$, $q_0 = \tan \phi_0 \sin \theta_0$ and θ_0 and ϕ_0 are the azimuth and zenith angles of the Sun. The reflectance map for a Lambertian reflectance function is

$$R(p,q) = (pp_0+qq_0+1) / (p^2+q^2+1^{1/2}(p_0^2+q_0^2+1)^{1/2}. \quad \text{(B1)}$$

Areas that face away from the Sun, i.e., where the numerator is negative are assigned zero reflectance.

It is assumed that the imaging sensor is far enough away for a parallel projection to hold. In particular, an oblique parallel projection is used [28]. For oblique viewing along the x axis, the point (x,y) is mapped to the point (x',y') where

$$x' = x\cos \phi_1 + z(x,y)\sin \phi_1$$
$$y' = y \quad \text{(B2)}$$

and ϕ_1 is the zenith angle of the sensor. That is, the surface is foreshortened only along the x direction. For viewing from another azimuth, the surface is simply rotated so that the line-of-sight is along the x axis. Since for $|\phi_1| > 0$, obscuration can occur, the hidden surfaces must first be removed. Then, the shaded rendition i(x,y) is mapped onto the image plane via Eq. (B2) and intermediate pixel locations are interpolated to obtain the projection i' (x',y').

Figure B2 summarises the fractal properties of images of the fractional Brownian surface shown in Fig. 1. The stability of the fractal dimension and model fit error over a wide range of illumination and viewing conditions implies that images of natural terrain are also fractal. It does not imply however that images containing man-made objects will not also be self-similar. For example, at low solar zenith angles where shading effects are reduced it may be difficult to discriminate man-made objects from the natural background. This phenomenon was noted in Section 4.

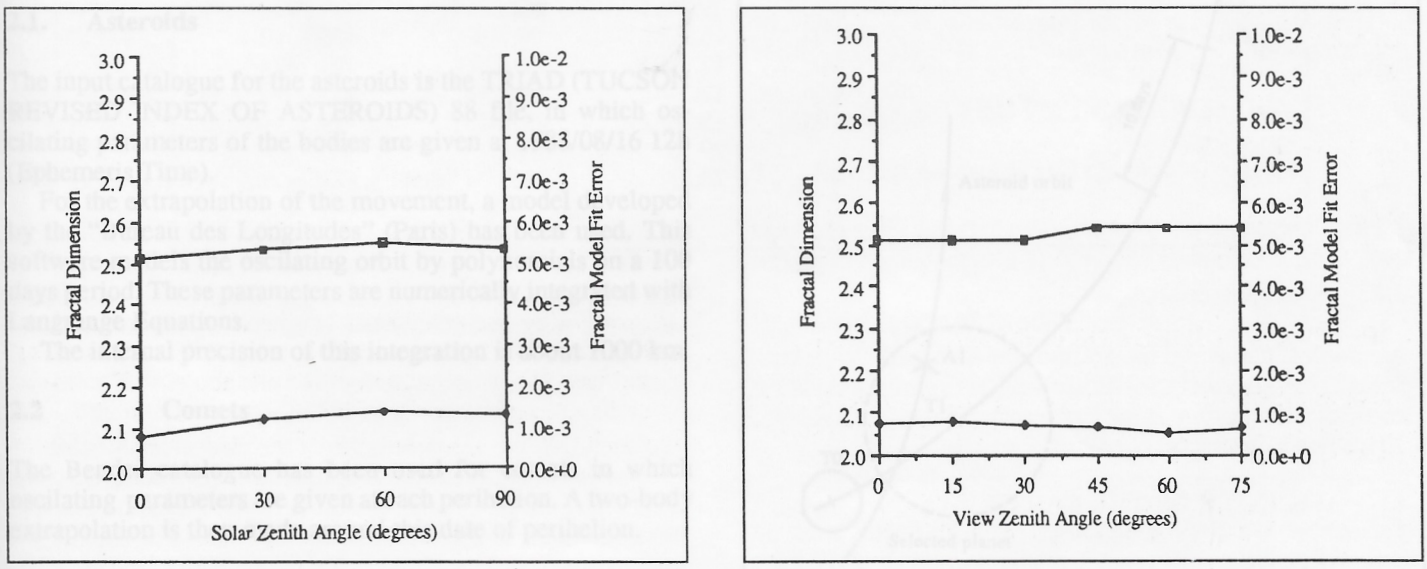

Fig. B2. Stability of fractal dimension and model fit as a function of Sun zenith (left) and view zenith (right) angle.

REFERENCES

1. F.D. Drake, "How can we detect radio transmissions from distant planetary systems?", in *Interstellar Communication*, A.G.W. Cameron (ed), W.A. Benjamin, New York, 1963.
2. J.Freeman and M.Lampton, "Interstellar archaeology and the prevalence of intelligence," *Icarus*, Vol 25, pp.368-369, 1975.
3. R.A. Freitas, "Extraterrestrial intelligence in the solar system: Resolving the Fermi Paradox," *JBIS*, **36**, pp.496-500, 1983.
4. G.Cocconi and P. Morrison, "Searching for interstellar communications," in *Interstellar Communication*, A.G.W. Cameron (ed), W.A. Benjamin, New York, 1963.
5. T.Denton, "Dancing in our lenses: Why there are not more technological civilisations," *JBIS*, **37**, pp..522-525.
6. R.A. Freitas, "If they are here, where are they? Observational and search considerations," *Icarus*, Vol. 55, pp.337-343, 1983.
7. M.D. Papagiannis, "The importance of exploring the asteroid belt," *Acta Astronautica*, Vol. 10, No.10, pp.709-712, 1983.
8. G.V. Foster, "Non-human artifacts in the solar system," ***Spaceflight***, Vol. 14, pp.447-453, December 1972.
9. V.DiPietro and G.Molenaar, *Unusual Martian Surface Features*, Mars Research, Glenn Dale, MD, 1982.
10. R. Pozos, *The Face on Mars: Evidence for a Lost Civilisation?*, North Atlantic Books, Berkeley, CA, 1986.
11. R. Hoagland, *The Monuments of Mars*, North Atlantic Books, Berkeley, CA, 1987.
12. M.J. Carlotto, "Digital image analysis of unusual Martian surface features," *Applied Optics*, Vol.27, pp.1926-1933, 1988.
13. B.B. Mandelbrot, *The Fractal Geometry of Nature*, W.H. Freeman, New York, 1983.
14. B.B. Mandelbrot and J.Van Ness, "Fractional Brownian motions, fractional noises and applications," *SIAM Review*, Vol.10, No. 4, pp.422-437, 1968.
15. D.M. Mark and P.B. Aronson, "Scale-dependent fractal dimensions of topographic surfaces: An empirical investigation, with applications in geomorphology and computer mapping," *Mathematical Geology*, Vol.16, No.7, 1984.
16. K.C. Clarke, "Scale-based simulation of topography," *Proceedings AutoCarto 8 (8th International Symposium on Computer-Assisted Cartography)*, Baltimore, MD, pp.680-688.
17. A. Woronow, "Morphometric consistency with the Hausdorff-Besicovitch dimension," *Mathematical Geology*, Vol.13, No.3, 1981.
18. R.F. Voss, "Random fractal forgeries," in *Fundamental Algorithms in Computer Graphics* (R.A. Earnshaw, ed), Springer-Verlag, Berlin, pp.805-835.
19. A. Fournier, D. Fussell, and L. Carpenter, "Computer rendering of stochastic models," *Communications of the ACM*, Vol. 25, No. 6, June 1982.
20. D.H. Ballard and C.M. Brown, *Computer Vision*, Prentice-Hall, Englewood Cliffs, NJ, 1982.
21. M.C. Stein, "Fractal image models and object detection", *Society of Photo-optical Instrumentation Engineers*, Vol.845, pp.293-300, 1987.
22. *Possibility of Intelligent Life Elsewhere in the Universe*, Report prepared for the Committee on Science and Technology US House of Representatives, October, 1977 (revised).
23. M.D. Papagiannis, "Conclusions and recommendations from the joint session on strategies for the search for life in the universe," in *Strategies for the Search for Life in the Universe*, M.D. Papagiannis (ed), D. Reidel Publishing, Dordrecht, Holland, 1980.
24. M.D. Papagiannis, "The Search for extraterrestrial life: recent developments. A report on IAU symposium 112," *JBIS*, Vol.38, pp.281-285, 1985.
25. A.P. Pentland, Fractal-based description of natural scenes," *IEEE Transactions on Pattern Analysis and Machine Intelligence*, Vol. 6, No. 6, November 1984.
26. P. Kube and A. Pentland, On the imaging of fractal surfaces," *IEEE Trans. PAMI*, Vol. 10, No. 5, September 1988.
27. B.K.P. Horn, "Hill shading and the reflectance map," *Proceedings of the IEEE*, Vol. 69, No. 1, January 1981.
28. J.D. Foley and A. Van Dam, *Fundamentals of interactive computer graphics*, Addison-Wesley, Reading, MA, 1983.

* * *